CORRELATION BETWEEN CHARACTERISTIC METEOROLOGICAL DROUGHT AND CLIMATE VARIABILITY IN GUNUNGKIDUL REGENCY USING SPI

Adyaksa Grahito Bagas Pamungkas[1], Astrid Damayanti[1]*, Riza Putera Syamsuddin[1]

[1]Department of Geography, Faculty of Mathematics and Natural Science, Universitas Indonesia, Depok, 16424, Indonesia

e-mail: astrid.damayanti@sci.ui.ac.id

Received: 14-01-2026 Revised: 16-01-2026; Approved: 31-03-2026

Abstract. Meteorological droughts act as the precursor to all other drought types, threatening food security and well-being. Meteorological droughts are closely related to rainfall that can be affected by climate variabilities such as El Nino Southern Oscillation (ENSO) and Indian Ocean Dipole (IOD), thus causing long drought conditions. Drought problems almost every year occur in Indonesia, including Gunungkidul Regency. Therefore, this study is expected to provide prevention of sustainable drought impacts and as a reference for further research. This study used data from a period of 30 years from 1991 to 2020 which included rainfall, sea level pressure (SLP), and sea surface temperature (SST). The Standardized Precipitation Index (SPI) was used in this study to characterize drought and classify drought levels with a time scale of 3 and 12 months. Climate variability was identified using the Southern Oscillation Index (SOI) for ENSO and the Dipole Mode Index (DMI) for IOD. Spatial descriptive analyses and statistical descriptive analyses are used to examine meteorological drought characteristics and patterns. Over the past 30 years, Gunungkidul Regency recorded more than 72 drought events. Meteorological droughts tend to occur in areas that have elevation between 200 – 400 masl, 0 – 200 masl, 400 – 600 masl, and >600 masl. The meteorological drought in Gunungkidul Regency will get worse if there is an El Nino and Positive IOD phase simultaneously.

Keywords: *ENSO, IOD, Gunungkidul Regency, meteorological drought, SPI.*

1 INTRODUCTION

Droughts are severe natural disasters that affect many areas of the world (Maybank et al., 1995). These events are typically characterized by a prolonged duration and a widespread spatial impact (Shi et al., 2022). Drought is generally classified into four categories: meteorological, agricultural, hydrological, and socioeconomic droughts (Arabameri et al., 2022; Saini et al., 2022; Tladi et al., 2022). Meteorological drought acts as the precursor to all other drought types. It is defined as a deficiency in precipitation over a large area spanning a prolonged period (Maybank et al., 1995), (Tladi et al., 2022). The primary driver of meteorological drought onset is a significant rainfall deficit (typically less than 75% of the average annual precipitation) (Abdulrazzaq et al., 2019; Anandharuban & Elango, 2021; Bhunia et al., 2020). Alterations in rainfall patterns and temperature regimes within ecosystems significantly increase the risk of plant mortality due to water stress (Carrière et al., 2020; Oliveira et al., 2021).

Droughts can severely compromise food security and human welfare

globally (Austin et al., 2021; Din et al., 2022; Tora et al., 2021). Prolonged drought conditions can even trigger human migration or displacement (WMO, 2006). In Indonesia, a significant portion of the archipelago experiences drought almost annually. Gunungkidul Regency is particularly vulnerable to these events (Sudaryatno, 2016). Drought vulnerability in Gunungkidul Regency is influenced by a combination of meteorological and geomorphological factors.

Gunungkidul Regency is primarily covered by the karst region. Karst region in Gunungkidul Regency has unique groundwater or certain characteristics (Ford & Williams, 1989; Z. Wang et al., 2022). Groundwater in Gunungkidul Regency is difficult to access due to its depth underneath the ground (Haryono et al., 2022). Consequently, local residents frequently rely on rainwater harvesting to meet their water demands (Maharani et al., 2022; Rahayu et al., 2022). The annual precipitation in Gunungkidul Regency ranges from 1,175 – 2,489 mm/year (Maharani et al., 2022). Climate variability such as El Nino Southern Oscillation (ENSO) and Indian Ocean Dipole (IOD) can affect precipitation in Gunungkidul Regency.

The ENSO phenomenon is closely linked to rainfall patterns in Indonesia (Lestari et al., 2018; Yulihastin et al., 2021). ENSO events can prolong the dry season or delay the onset of the rainy season (Kurniadi et al., 2021; Nurdiati et al., 2022). In addition to ENSO, the IOD also influences precipitation patterns (Lestari et al., 2018; Zhang et al., 2022). The process of ocean interaction with the atmosphere by the IOD can affect the pattern of rainfall anomalies in the tropics through teleconnection between the oceans and the atmosphere (Narulita et al., 2021; Nurdiati et al., 2022). The simultaneous occurrence of El Nino and Positive IOD phenomena can affect seasonal and annual rainfall deficits (Amirudin et al., 2020; Kurniadi et al., 2021; Mubarrok & Jang, 2022; Narulita et al., 2021; Saji & Yamagata, 2003; Siswanto et al., 2022; Yin et al., 2022).

Effective monitoring is essential to mitigate the risk of drought and its consequent adverse effects. This study evaluated meteorological drought patterns using rainfall data spanning from 1991 to 2020. The Standardized Precipitation Index (SPI) was utilized to quantify the duration, magnitude, severity, frequency, and intensity of meteorological drought (Bhunia et al., 2020; Bong & Richard, 2020; Caloiero et al., 2021; McKee et al., 1993). SPI can be applied for multi-time scales (1, 2, 3, 6, 9, and 12 months) (Bhunia et al., 2020; Qaisrani et al., 2021; Salimi et al., 2021; Wu et al., 2021). In this study adopted the 3 and 12-months scales to capture short dan long term drought characteristics.

ENSO events can be identified using the Southern Oscillation Index (SOI) (Nugroho et al., 2021; Ropelewski & Halpert, 1989). The SOI is calculated based on sea level pressure (SLP) difference between Tahiti and Darwin (Araneda-Cabrera et al., 2021; Feng et al., 2022; Odériz et al., 2020; Raut et al., n.d.; Ropelewski & Halpert, 1989; Trenberth, 1984). IOD events can be identified through the Dipole Mode Index (DMI) (Nurdiati et al., 2022; Saji et al., 1999). The DMI represents the difference in sea surface temperature (SST) anomalies between the western Indian Ocean (50° – 70° E, 10° N – 10°S) and eastern Indian Ocean (90° – 110° E, 10° S – 0°) (Saji et al., 1999). The objective of this study is to quantify the severity of meteorological drought in Gunungkidul Regency and to assess the influence of ENSO and IOD on these drought events.

2 MATERIALS AND METHODOLOGY

2.1 Study Area

Musi The study was conducted in Gunungkidul Regency, Special Region Yogyakarta. Gunungkidul Regency is located between 7°46'00" S – 8°09'00" S and 110°21'00" E – 110°50'00" E, covering a total area of about 1,485.36 km^2. The study area consists of 18 sub-regencies, and Wonosari sub-regency is the capital of Gunungkidul Regency **(Fig.2-1)**.

The topography of the study area is characterized by a general descent towards the center, with approximately 94% of the region situated at an elevation between 0 and 400 meters

above sea level (masl). Karst landscapes cover an estimated 807 km², accounting for 53% of Gunungkidul Regency. This karst region constitutes part of the broader Gunung Sewu Karst Area, extending across the regency from west to east. Bordered by the Indian Ocean to the south, the area possesses distinct physical features, including the Nglanggeran Ancient Volcano, extensive underground river systems, and numerous caverns. The region experiences annual precipitation ranging from 1,175 to 2,489 mm/year, with temperatures varying between 17.3°C and 35.5°C (Maharani et al., 2022). Persistent water scarcity remains a critical impediment to economic development in Gunungkidul Regency, a challenge exacerbated by population growth, industrialization, and agricultural expansion.

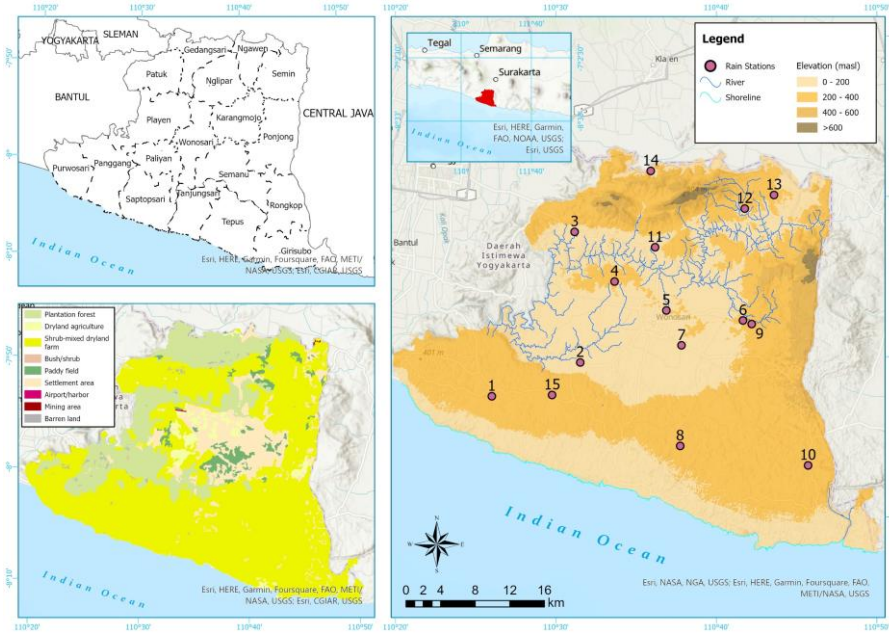

Fig. 2-1 Distribution of the rain stations, elevation, geographic location, and land cover in Gunungkidul Regency

2.2 Data

The daily precipitation dataset for this study was gathered from 15 rainfall stations **(Table 3-2)**. Rainfall data from 1991 to 2020 for all stations are provided by The Department of Agriculture and Food, Gunungkidul Regency. The spatial distribution of daily rainfall data has been converted into average monthly data. Climate variability data such as El-Nino Southern Oscillation (ENSO) have been acquired from (http://www.bom.gov.au/climate/enso/soi/) the website of the Australian Government Bureau of Meteorology and Indian Ocean Dipole (IOD) have been acquired from the website of National Oceanic and Atmospheric Administration (NOAA) (https://psl.noaa.gov/gcos_wgsp/Timeseries/DMI/). The Indonesian Geospatial Information Agency's Digital Elevation Model Nasional (DEMNAS) is used in the study. IfSAR data (5 m resolution), TERRASAR-X (5 m resolution), ALOS - PALSAR (11.25 m resolution), and the addition of mass point data to the results of stereo plotting were used to develop DEMNAS (BIG, 2018). DEMNAS has a high spatial resolution about 0.27 arcsecond for procuring the elevation of all stations.

2.3 Method

A. The Complete and test the consistency of rainfall data

Long-term rainfall data were retrieved from 15 monitoring stations spatially distributed across Gunungkidul Regency **(Fig.2-1)**. While the primary dataset spans a 30-year period, distinct temporal coverages were noted for specific stations. two stations possess records spanning approximately 25-years, while two others cover a 23-year period. Incomplete rainfall records were imputed using the Inverse

Distance Method. This approach utilizes the distance between rainfall stations as a weighting factor, where the influence of neighboring stations diminishes as the distance increases (de Silva et al., 2007; Djerbouai, 2022; Mohamed Salleh et al., 2021). For this study, the method was configured with a power parameter (p) of two and utilized data from the nearest three stations to ensure local spatial representativeness. The estimation is governed by the following equation:

$$P_x = \frac{\sum_{i=1}^{n} \frac{1}{d^2} P_i}{\sum_{i=1}^{n} \frac{1}{d^2}} \quad (1)$$

where is P_x estimate of rainfall for the ungauged station; P_i is rainfall values of rain gauges used for estimation, d_i is distance from each location the point being estimated, n is number of surrounding stations.

Rainfall data consistency test in this study using Rescaled Adjusted Partial Sums (RAPS) Method (Huang et al., 2021; Jenifer & Jha, 2021; Suhartanto et al., 2021). A RAPS based visualization approach overcomes modest systematic changes in records as well as variability in data values itself. The RAPS visualization reveals periodicities, irregular fluctuations, data clustering, trends, and shifts in the record. (Garbrecht & Fernandez, 1994). The RAPS Method is calculated by using the following equation:

$$X_k = \sum_{t=1}^{k} \frac{Y_t - \bar{Y}}{S_Y} ; k = 1, \dots, n \quad (2)$$

where is $\bar{Y}$ sample mean; SY2 is variance; n is number of values in the time series; k is counter limit of the current summation. The plot of the RAPS versus time is the visualization of the trends and fluctuations of Yt.

The consistency of the rainfall datasets was evaluated using the RAPS method. The results confirmed that the test statistics for all 15 stations remained within the 95% confidence limits, indicating that the data are homogeneous and suitable for further analysis.

B. Classify SOI and DMI

The Southern Oscillation Index (SOI) shows how El Nino or La Nia events develop and how intense they are in the Pacific Ocean (Bagale et al., 2021; Emmanuel, 2022; J. Li et al., 2021; Nugroho et al., 2021; Ropelewski & Halpert, 1989). The SOI is determined by calculating using the pressure differences between Tahiti and Darwin. La Nina events are frequently indicated by the SOI showing continuously positive values +7. El Nino events are frequently indicated by the SOI showing continuously negative values -7. ENSO development occurs in three phases: the onset period from March to June, the peak period from July to December, and the decay period from January to April. The El Nino development onset period started in March-April-May (MAM) (Harrison & Larkin, 1998).

IOD intensity is represented by an abnormal SST gradient between the south-eastern Indian Ocean (50° - 70° E and 10° S - 10° N) and western equatorial Indian Ocean (90° - 110° E and 10° S - 0° N). This gradient is known as the Dipole Mode Index (DMI). When the DMI is positive, the phenomenon is referred to as the positive IOD, and when it is negative, it is referred to as the negative IOD. IOD index is neutral when IOD shows values between −0.4°C and +0.4°C (Agustina et al., 2021; Cahyarini et al., 2021; H. Li et al., 2022).

C. Drought indices

SPI is a meteorological drought index created by McKee et al (1993). With this index, wet and dry occurrences in an area can be assessed. The characteristics of drought include duration, magnitude, severity, intensity, and frequency. It is a widely used indicator for measuring drought occurrences due to its ease of use (based on precipitation). The SPI calculation utilizes multiple time scales (1, 3, 6, 9, and 12 months) (Bhunia et al., 2020; Qaisrani et al., 2021; Salimi et al., 2021; Wu et al., 2021). A more objective assessment of dry and wet periods is possible through the gamma-modeling of historical data and the transformation of gamma-modeled data to normally distributed data. These steps are used to calculate a SPI (Ali et

al., 2011; Bhunia et al., 2020; W. Wang et al., 2021):

The previous j months where time scales (1, 3, 6, and 12 months) used to generate a set of averaging periods (Qaisrani et al., 2021; Salimi et al., 2021; Wu et al., 2021). The relationship between the probability and the rainfall was determined by fitting each data set to the gamma function. The probability density function of the gamma distribution is given by

$$g(x) = \frac{1}{\beta^{\alpha}\Gamma(\alpha)} x^{\alpha-1} e^{-x/\beta}, x > o \quad (3)$$

where α are shape and β are scale parameters. x is the amount of precipitation, and $\Gamma(\alpha)$ is the gamma function. α and β are required to be estimated for fitting the distribution to the data for each timesteps of interest for each rainfall station.

The maximum likelihood method by Thom (1958) was applied to estimate scale and shape parameters as below:

$$\hat{\alpha} = \frac{1}{4A}\left(1 + \sqrt{1 + \frac{4A}{3}}\right) \text{ and } \hat{\beta} = \frac{\bar{x}}{\hat{\alpha}} \quad (4)$$

with

$$A = \ln(\bar{x}) - \frac{\sum \ln(x)}{n} \quad (5)$$

Where $\bar{x}$ represents the average precipitation; n represents the numbers of data point in the series; x represents the precipitation at the current period.

The cumulative probability of an observed amount of precipitation is calculated using the equation in the following step:

$$G(x) = \int_0^x g(x)dx = \frac{1}{\hat{\beta}^{\hat{\alpha}}\Gamma(\hat{\alpha})} \int_0^x x^{\hat{\alpha}-1} e^{-x/\hat{\beta}}\, dx \quad (6)$$

When x = 0, the gamma distribution will return an undefined value. Therefore, the above question is modified as shown below

$$H(x) = q + (1-q)G(x) \quad (7)$$

After estimating the modified cumulative probability, an approximation of the SPI index can be computed.:

$$SPI = \begin{cases} -\left(t - \frac{C_0 + C_1 t + C_2 t^2}{1 + d_1 t + d_2 t^2 + d_3 t^3}\right), 0 < H(x) \leq 0{,}5 \\ +\left(t - \frac{C_0 + C_1 t + C_2 t^2}{1 + d_1 t + d_2 t^2 + d_3 t^3}\right), 0{,}5 < H(x) < 1 \end{cases} \quad (8)$$

where

$$a = \begin{cases} \sqrt{ln\left(\frac{1}{(H(x))^2}\right)}, 0 < H(x) \leq 0{,}5 \\ \sqrt{ln\left(\frac{1}{(1{,}0 - H(x))^2}\right)}, 0{,}5 < H(x) < 1 \end{cases} \quad (9)$$

And c_0 = 2.515517, c_1 = 0.802853, c_3 = 0.010328, d_1 = 1.432788, d_2 = 189269, dan d_3 = 0.001308.

The SPI classification in eight categories, as shown in **Table 2-1**.

TABLE 2-1. classification of the spi value

Classification	Value
Extremely wet	SPI ≥ 2
Very wet	1.5 ≤ SPI < 2
Moderately wet	1 ≤ SPI < 1.5
Near normal	-1 < SPI < 1
Moderately dry	-1.5 < SPI ≤ -1
Severely dry	-2 < SPI ≤ -1.5
Extremely dry	SPI ≤ -2

In this study, SPI values were calculated using the SPI Program software from the National Drought Mitigation Center (NDMC), University of Nebraska-Lincoln. The Run Theory concept, developed by Yevjevich (1967) and Dracup et al. (1980), was adopted to identify drought characteristics at each rainfall station **(Fig. 2-2)**.

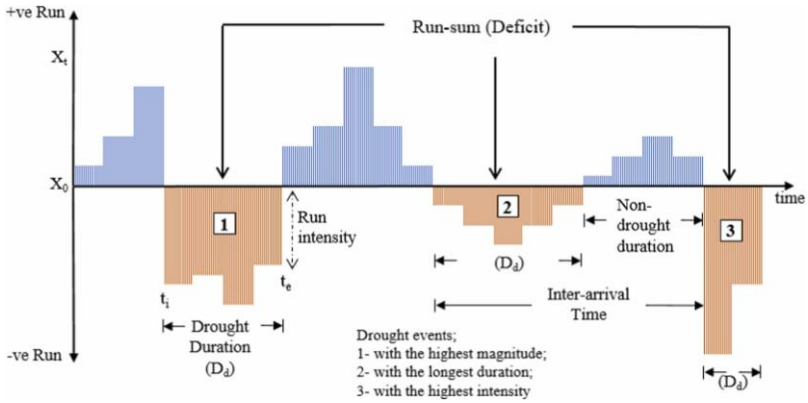

Fig. 2-2 Concept of run theory for a given threshold level

According to this method, a drought event initiates when X_t (SPI) is continuously less than zero (X_0) and reaches an intensity of -1 or less, terminating when X_t becomes positive. The duration (or run-length) is defined as the period between the start (t_i) and end (t_e) of the drought; consequently, the reported drought event counts refer to the cumulative number of months exhibiting drought conditions. The magnitude (or run-sum) represents the cumulative water deficit (*e.g.*, rainfall deficiency) during the event. Drought intensity is calculated by dividing the magnitude by the duration (Yildirim et al., 2022). Drought frequency is the proportion of drought that occurred during the observation period (total value of drought duration divided by total number of months) (Mohseni Saravi et al., 2009).

Drought severity refers to the drought classifications based on SPI **(Table 2-1)** (Bong & Richard, 2020; McKee et al., 1993). To characterize drought conditions across the entire research area, these station-based drought metrics were subsequently interpolated using the spatial methods. Finally, descriptive statistical analysis was applied to evaluate the overall drought indicators.

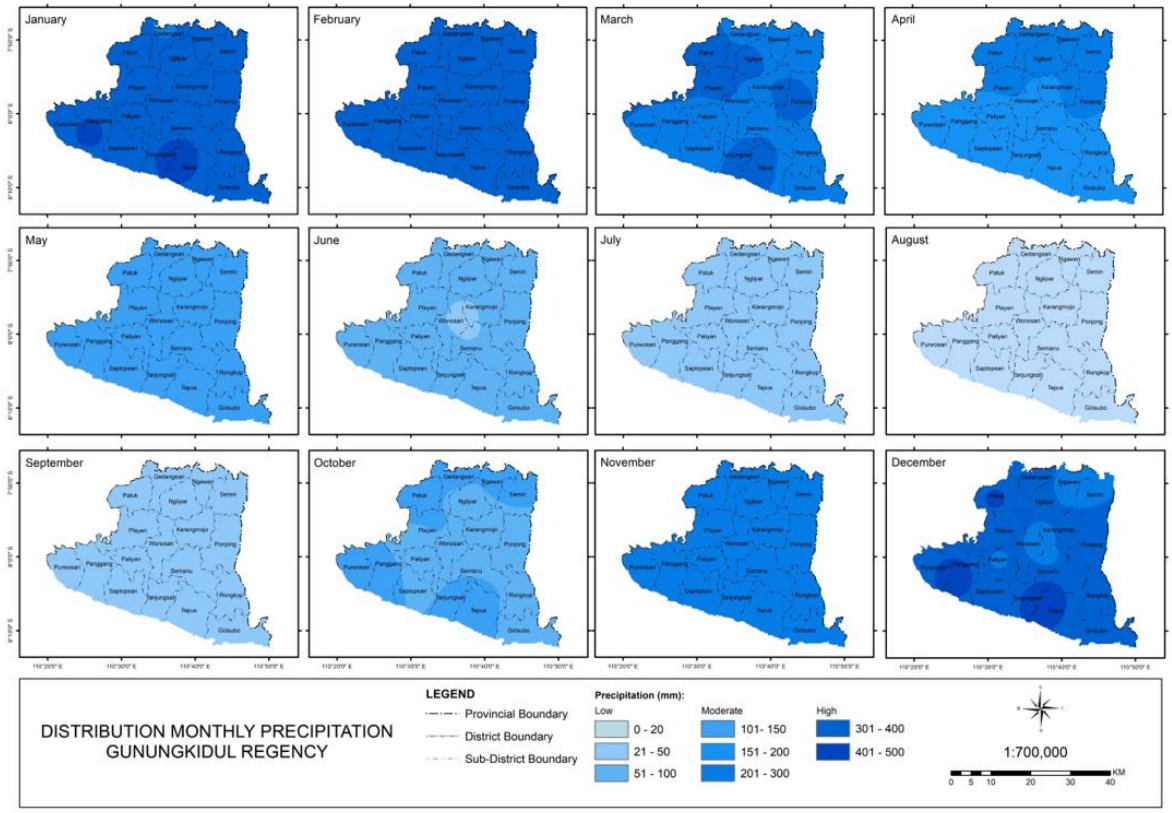

Fig. 2-3 Map distribution monthly rainfall in Gunungkidul Regency

D. Composition of spatial maps

To illustrate the spatial distribution of precipitation and severity level of drought, the spline interpolation technique was employed (Ali et al., 2011; Yildirim & Rahman, 2022). This surface estimation model has been continuously improved over the decade and is recognized for its mathematical robustness. By minimizing the function that combines the mean square residuals and the roughness of the signal surface, the model effectively smooths the data (Mazhar & Nawaz, 2014).

By minimizing the function that combines the mean square residuals and the roughness of the signal surface, the model effectively smooths the data (Mazhar & Nawaz, 2014). The spline interpolation was computed using ArcGIS Pro 3.0.2 software.

E. The correlation analysis

Table 2-2. classification of the pearson correlation coefficient

Classification	Value
Very weak correlation	0.0 – 0.2
Weak correlation	0.2 – 0.4
Moderate correlation	0.4 – 0.6
Strong correlation	0.6 – 0.8
Very strong correlation	0.8 – 1.0

The Pearson Correlation Coefficient (PCC) developed by Pearson (1895), has been widely used throughout correlation analysis (Z. Wang et al., 2022). In this study, PCC used to identify the correlation between SPI 3 months and SOI and DMI. The correlation coefficient varies from -1 to 1, where -1, 0, and 1 represent a negative correlation, no correlation, and positive correlation (Du et al., 2022; Elhoussaoui et al., 2021; Evans, 1996; Khoi et al., 2021). The correlate action coefficient's absolute value was used to calculate the degree of correlation **(Table 2-2)**.

3 RESULTS AND DISCUSSION

In this study, 15 rain stations in the Gunungkidul Regency were filled, calibrated, and used to generate rainfall data. The results were consistent among all 15 rain stations. Fig. 2-3 illustrates that precipitation in Gunungkidul Regency is highest at the beginning and end of the year, while it tends to be lowest in the middle of the year. The monthly rainfall trend in Gunungkidul indicates that the greatest rainfall occurs in January, then drops in February to its lowest peak in August. It started increasing in September and continued until December. Monthly precipitation data could describe a pattern of rapidly growing precipitation in the South and North, which are located at elevations more than 200 masl. This indicates that precipitation in Gunungkidul Regency can be affected by elevation.

3.1 *ENSO and IOD events*

According to the **Fig 3-1**, La Nina events include 1998, 1999, 2010, and others, whereas El Nino events include 1994, 1997, 2015, and others. Negative IOD events occurred in 1992 and 1995, whereas positive IOD events occurred in 1997 and 2015. In 1997/1998, the SOI value was negative and ranged from -8.5 to -28.5. The DMI value during that year was positive and ranged from 0.5 to 0.54. El Nino occurred from March 1997 until April 1998, and the positive IOD occurred from July 1997 to February 1998.

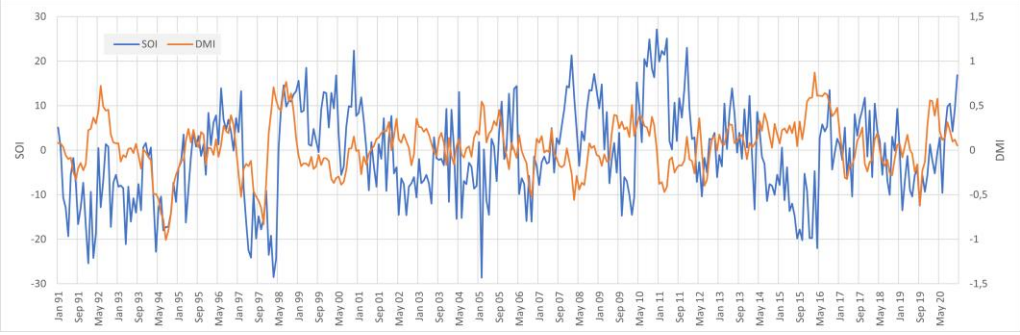

Fig. 3-1 Monthly data SOI and SPI 1991 – 2020

3.2 Meteorological drought characteristic

The SPI value can be used to assess meteorological droughts. These values indicate the following results: drought duration (DD), drought magnitude (DM), drought severity (DS), drought frequency (DF), and drought intensity (DI). The length of a drought event is determined by assessing it from the start of the month (including) to the end of the month (excluding). The sum of the determined SPI values or severity values throughout all drought durations is the drought magnitude. The severity of the drought will worsen as its magnitude decreases. Gunungkidul Regency has suffered droughts of various durations and magnitudes over the last 30 years. Gunungkidul Regency suffers drought on average for 5 months (SPI 3) and 22 months (SPI 12). Average drought magnitudes for the Gunungkidul Regency from 1991 – 2020 were -5.29 for the SPI 3 and -26.29 for the SPI 12. The drought duration and magnitude for each rain station, as shown in **Table 3-2**.

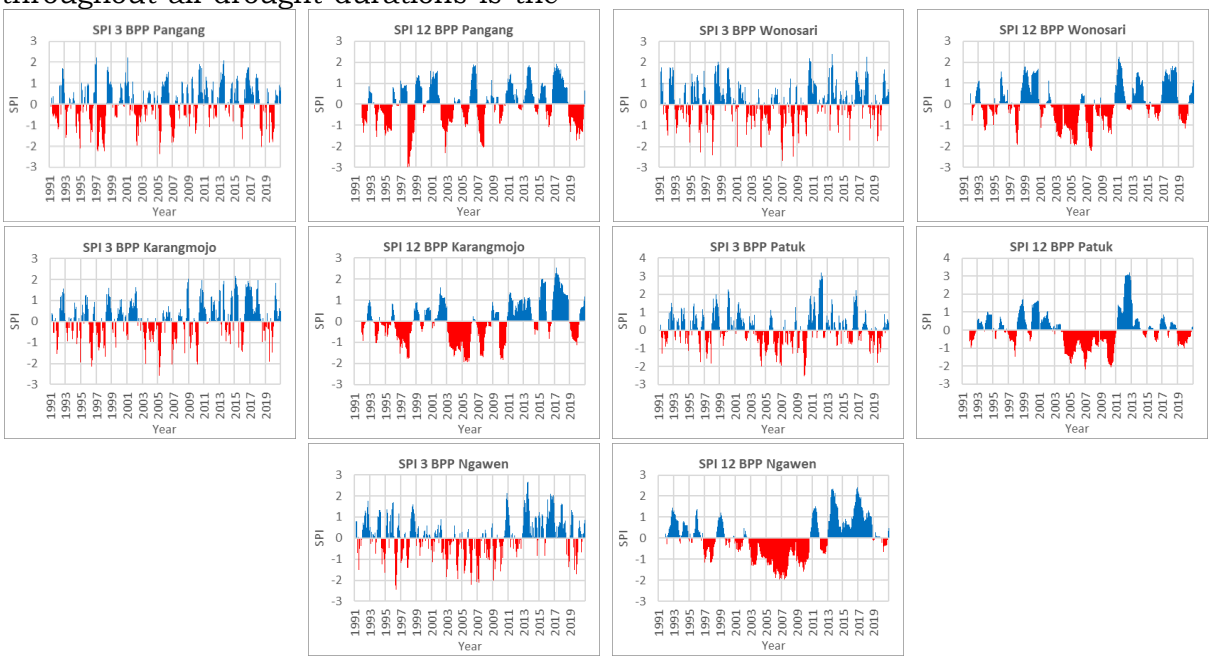

Fig. 3-2 SPI 3 and SPI 12 value for each rain station categories

Rain station in Gunungkidul Regency can be classified into five categories based on its region and elevation. Five categories are the southern with elevation 200 – 400 masl, the central region with elevation 0 – 200 masl, the central region with elevation 200 – 400 masl, the north with elevation 0 – 200 masl, and north with elevation 200 – 400masl. There are four rain stations in the southern part of the Gunungkidul Regency including BPP Panggang, BPP Rongkop, BPP Tepus, and BPP Saptosari. There are six rain stations in the Gunungkidul Regency's central region. BPP Wonosari, BPP Paliyan, and BPP Semanu are a few of the central region's rain stations, which are all located at an elevation 0 – 200 masl. BPP Playen, BPP Karangmojo, and BPP Ponjong are rain stations that are located at elevations 200 – 400 masl. There are five rain stations in the north. BPP Gedangsari, BPP Nglipar, and BPP Patuk are a few northern rain stations that are placed 0 – 200 masl, whereas BPP Semin and BPP Ngawen are located above that elevation.

Fig. 3-1 illustrates the drought severity as the monthly calculated value of the SPI 3 and SPI 12 for each rain station categories. Drought occurs when the SPI value is below -1 and end when the SPI value is positive. Drought that has a long duration is shown when the SPI value is below -1 in a row, whereas the extremely dry drought is indicated at the lowest SPI value or the SPI value less than -2. The lowest SPI value among all rain stations is -2.99. This value occurred in December 1997 at BPP Panggang. The longest drought and

extremely dry drought, as shown in Table 5. The spatial pattern of the extremely dry drought in Gunungkidul Regency 1997 and 2019, as shown in Fig. 3-3.

TABLE 3-1
THE SEVERITY OF METEOROLOGICAL DROUGHT BASED ON THE ELEVATION 1991 - 2020

Severity Drought	Elevation (masl)			
	0 – 200	200 – 400	400 – 600	>600
Moderately Dry	16	18	13	8
Severe Dry	13	14	8	5
Extremely Dry	5	4	3	3
Total	34	36	24	16

In the past 30 years (1991 – 2020), meteorological droughts based on elevation have a tendency to occurred 36 times at 200 - 400 masl, 34 times at 0 - 200 masl, 24 times at 400 - 600 masl, and 16 times at >600 masl. The severity of the meteorological drought based on the elevation of the region in Gunungkidul Regency is shown in **Table 3-1**.

Agriculture in Gunungkidul Regency may be affected by a meteorological drought. Tubers are a type of dry land agriculture that commonly survives in dry periods such as 2009 and 2010. Agricultural production tends to rise during normal or wet periods in 2011 and 2012. Increased agricultural products, such as rice plants.

According to the SPI 3 value, BPP Panggang had the highest proportion of drought for the past 30 years (24.44%), while BPP Nglipar had the lowest (15.56%). BPP Semin (15.06%) has the lowest proportion of droughts lasting fewer than 30 years. Except for BPP Nglipar (15.56%), all of the rain stations in Gunungkidul Regency with 30 years of data show that more than 18% of the proportion is in a drought. A significant proportion of Gunungkidul Regency's areas have therefore suffered drought for at least 60 months during a period of 360 months (30 years).

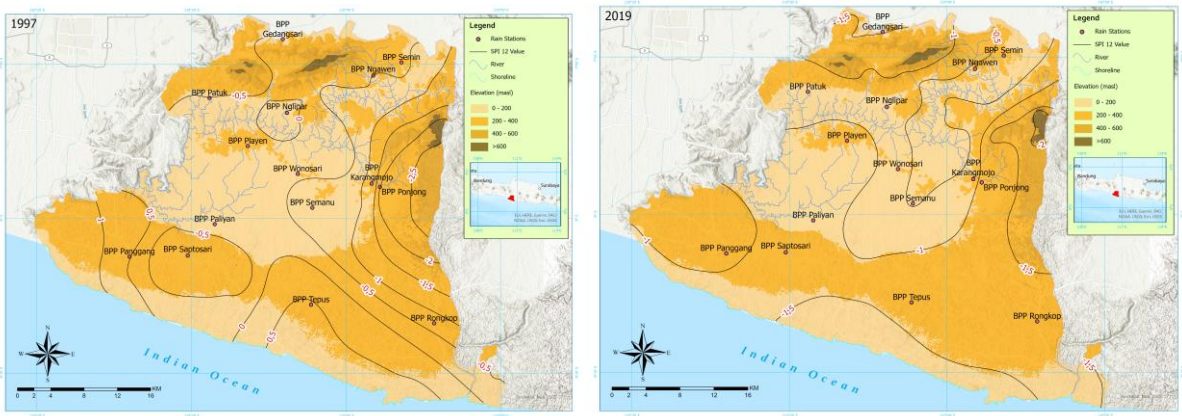

Fig. 3-3 SPI 12 value in Gunungkidul Regency 1997 and 2019

According to SPI 12 value, BPP Rongkop had the highest proportion of droughts during the past 30 years (33.33%), whereas BPP Tepus had the lowest proportion (21.39%). BPP Saptosari (35.76%) and BPP Semin (11.22%) had the highest and lowest percentages of droughts lasting fewer than 30 years. Commonly, the proportion of drought is approximately 20 – 30% for rain stations with other 30-year data. According to SPI 12, a significant proportion of Gunungkidul Regency's areas suffered drought for at least 72 months over a 360-month period (30 years). The drought frequency Gunungkidul Regency 1991 – 2020, as shown in **Table 3-2**.

Drought intensity is the ratio of drought magnitude to duration. The intensity value of the drought reflects the level of drought in the study area. This indicate is required because a significant number of droughts occur in a short period yet have a high intensity of drought severity, or vice versa. In Gunungkidul Regency, the average drought intensity value is respectively -1.14 (SPI 3) and -1.16 (SPI 12) **(Table 3-2)**.

The SPI 3 indicates the intensity of the 15 rain stations, of which two have intensities from 0 to -1, nine have intensities from -1 to -1.2, and four have intensities below -1.2. This indicates that the drought is more severe at the four rain stations (BPP Ponjong, BPP Rongkop, BPP Nglipar, and BPP Semin) than it is at the other rain stations. The SPI 12 indicates the intensity of the 15 rain stations that are occurring drought, two of which have intensity values from 0 to -1. The two stations are BPP Tepus and BPP Ponjong. Ten stations had intensity values between -1 to -1.2. Three stations then had intensity values greater than -1.2. BPP Semanu, BPP Ponjong, and BPP Semin are the three stations.

3.3 Correlation between climate variability and meteorological drought

ENSO and IOD can affect rainfall (Kurniadi et al., 2021). A meteorological drought occurs when rainfall is below normal (Bhunia et al., 2020; Narulita et al., 2021). ENSO's influence on the decrease in the intensity of rainfall occurs during the El Nino phase. At this phase, the temperature of the western Pacific Ocean is lower than the middle and east, which results in a slower rainy season or a longer dry season. IOD can also affect the intensity of rainfall during the positive IOD phase. At this phase, the sea level temperature in the eastern Indian Ocean is low compared to the west, which causes the region in Indonesia to be dry. Positive IOD events can strengthen or worsen the drought caused by ENSO in the maritime archipelago (Lestari et al., 2018), as was the case in 1997–1998.

Table 3-2. Characteristic meteorological drought in gunungkidul regency

No	Rain Station	Elevation (masl)	Range Data	Duration (month)				Magnitude				Frequency		Intensity	
				SPI 3	AvD SPI 3	SPI 12	AvD SPI 12	SPI 3	AvM SPI 3	SPI 12	AvM SPI 12	SPI 3	SPI 12	SPI 3	SPI 12
1	BPP Panggang	299	1991 - 2020	88	6	101	11	-98.69	-6.58	-116.49	-12.94	24.44%	28.06%	-1.12	-1.15
2	BPP Paliyan	165	1991 - 2020	83	4	104	17	-86.59	-4.56	-123.07	-20.51	23.06%	28.89%	-1.04	-1.18
3	BPP Patuk	130	1991 - 2020	82	7	85	21	-79.53	-6.63	-93.63	-23.41	22.78%	23.61%	-0.97	-1.10
4	BPP Playen	204	1991 - 2020	69	5	117	20	-75.24	-5.02	-107.37	-17.90	19.17%	32.50%	-1.09	-0.92
5	BPP Wonosari	200	1991 - 2020	82	4	104	15	-85.86	-3.90	-105.92	-15.13	22.78%	28.89%	-1.05	-1.02
6	BPP Karangmojo	208	1991 - 2020	67	4	97	16	-79.02	-4.39	-107.86	-17.98	18.61%	26.94%	-1.18	-1.11
7	BPP Semanu	190	1991 - 2020	71	4	79	20	-84.26	-5.27	-99.28	-24.82	19.72%	21.94%	-1.19	-1.26
8	BPP Tepus	253	1991 - 2020	87	6	77	13	-79.68	-6.13	-71.68	-11.95	24.17%	21.39%	-0.92	-0.93
9	BPP Ponjong	210	1995 - 2020	56	6	64	16	-70.18	-7.02	-92.66	-23.17	17.95%	20.51%	-1.25	-1.45
10	BPP Rongkop	308	1991 - 2020	66	4	120	17	-83.78	-4.93	-127.28	-18.18	18.33%	33.33%	-1.27	-1.06
11	BPP Nglipar	167	1991 - 2020	56	4	97	32	-68.71	-4.91	-107.21	-35.74	15.56%	26.94%	-1.23	-1.11
12	BPP Ngawen	209	1991 - 2020	81	4	109	55	-89.41	-4.71	-120.04	-60.02	22.50%	30.28%	-1.10	-1.10
13	BPP Semin	207	1995 - 2020	47	5	35	35	-64.09	-6.41	-63.85	-63.85	15.06%	11.22%	-1.36	-1.82
14	BPP Gedangsari	138	1997 - 2020	59	4	81	20	-67.64	-4.23	-90.05	-22.51	20.49%	28.13%	-1.15	-1.11
15	BPP Saptosari	300	1997 - 2020	57	4	103	26	-65.43	-4.67	-104.85	-26.21	19.79%	35.76%	-1.15	-1.02

In 1997-1998, the SOI value was below -7 for 14 consecutive months. According to Harrison and Larkin (1998) onset period of the ENSO development cycle, the development of El Nino in 1997 began in March. In 1997/1998, the SOI value dropped to -28.5 in March 1998. Along with the development of ENSO, IOD occurred in 1997–1998. The development of a positive IOD in 1997 began in July. For the past eight months, the DMI value has been greater than +0.4. The DMI value during 1997–1998 reached its highest value of 1.40 in November 1997. The SPI-3 value during the development of ENSO and IOD in 1997–1998 at each rain post was very diverse.

In March 1997, the SPI 3 value in BPP Panggang and BPP Ponjong was very low below -2. The SPI 3 value in both rain posts was below -2 for three consecutive months. In July 1997, the value of SPI 3 on each rain posts ranged from 0 to -1.39. The SPI 3 value of this month is not as low as in March 1997. In November 1997, the SPI 3 value in BPP Ponjong touched a figure below -2. SPI 3 for the month averages -1.59. In March 1998, the SPI 3 value for this month averaged 0.56. SPI 3 values tend to be low when the SOI value is low and the DMI value is high, such as in November, December, and January 1997/1998. The relationship between the SOI value and the DMI value with SPI 3 can analyze with pearson correlation

Table 3-3. Drought longest and extremely dry in gunungkidul regency based spi 12 value

No	Rain Stations	Drought longest (≤ -1)			Drought extremely dry (≤ -2)		
		DD	Date	DM	DD	Date	DM
1	BPP Panggang	23	Jan, 2019 - Dec, 2020	-24.45	11	Dec, 1997 - Nov, 1998	-22.22
					14	Oct, 2002 - Dec, 2003	-14.55
					5	Sep, 2007 - Feb, 2008	-6.45
2	BPP Paliyan	46	May, 2002 - Mar, 2006	-65.62	10	Feb, 1998 - Dec, 1998	-10.85
					41	Oct, 2002 - Mar, 2006	-58.1
3	BPP Patuk	54	May, 2004 - Nov, 2008	-62.32	23	Dec, 2006 - Nov, 2008	-24.4
					10	Apr, 2010 - Feb, 2011	-12.24
4	BPP Playen	35	Feb, 2005 - Jan, 2008	-30.19	10	May, 2016 - Mar, 2017	-14.26
5	BPP Wonosari	37	Feb, 2003 - Mar, 2006	-47.37	8	May, 2007 - Jan, 2008	-14.14
6	BPP Karangmojo	36	May, 2003 - May, 2006	-48.89		-	
7	BPP Semanu	39	Jan, 2003 - Apr, 2006	-44.3	23	May, 2007 - Apr, 2009	-38.55
8	BPP Tepus	36	Sep, 2002 - Sep, 2005	-35.29		-	
9	BPP Ponjong	22	Dec, 1996 - Sep, 1998	-35.65	12	Oct, 1997 - Sep, 1998	-18.58
		22	Feb, 2019 - Dec, 2020	-30.73			
10	BPP Rongkop	35	Apr, 2003 - Mar, 2006	-29.26	9	Jan, 1998 - Sep, 1998	-9.72
					8	Jun, 2007 - Feb, 2008	-13.23
					7	Apr, 2010 - Nov, 2010	-10.4
11	BPP Nglipar	82	Mar, 2004 - Jan, 2011	-96.86	70	Mar, 2005 - Jan, 2011	-77.21
12	BPP Ngawen	92	Feb, 2003 - Oct, 2010	-107.46		-	
13	BPP Semin	35	Dec, 2004 - Nov, 2007	-63.85	35	Dec, 2004 - Nov, 2007	-63.85
14	BPP Gedangsari	44	Jan, 2007 - Sep, 2010	-53.59	23	Dec, 2018 - Nov, 2020	-28.87
15	BPP Saptosari	45	Mar, 2007 - Des, 2010	-44.29	13	Mar, 2005 - Apr, 2006	-22.05

TABLE 3-4
Pearson correlation coefficients between spi 3 and climate indices for each station.

Rainfall Station	Data Duration (Years)	N (Months)	SOI Correlation (r)	SOI Sig. (p-value)	DMI Correlation (r)	DMI Sig. (p-value)
BPP Panggang	30	360	0.434	< 0.001	-0.370	< 0.001
BPP Paliyan	30	360	0.393	< 0.001	-0.301	< 0.001
BPP Patuk	30	360	0.268	< 0.001	-0.291	< 0.001
BPP Playen	30	360	0.311	< 0.001	-0.343	< 0.001
BPP Wonosari	30	360	0.303	< 0.001	-0.297	< 0.001
BPP Karangmojo	30	360	0.283	< 0.001	-0.275	< 0.001
BPP Semanu	30	360	0.329	< 0.001	-0.279	< 0.001
BPP Ponjong	26	312	0.228	< 0.001	-0.395	< 0.001
BPP Tepus	30	360	0.234	< 0.001	-0.404	< 0.001
BPP Rongkop	30	360	0.359	< 0.001	-0.368	< 0.001
BPP Nglipar	30	360	0.165	0.002	-0.301	< 0.001
BPP Ngawen	30	360	0.134	0.011	-0.296	< 0.001
BPP Semin	26	312	0.169	0.003	-0.202	< 0.001
BPP Gedangsari	24	288	0.087	0.143	-0.364	< 0.001
BPP Saptosari	24	288	0.363	< 0.001	-0.366	< 0.001

The Pearson correlation was used to assess the correlation between SOI and DMI on SPI values. The sig row (2-tailed) is used to determine significance. A correlation is deemed significant if the value of significant (Sig. 2-tailed) is less than 0.05. The Pearson correlation analysis, summarized in **Table 3-4**, elucidates the relationship between meteorological drought (SPI-3) and large-scale climate indices. The results demonstrate a predominantly positive and statistically significant correlation between SPI 3 and the SOI across the majority of stations ($p < 0.05$), with the notable exception of BPP Gedangsari ($p = 0.143$). This positive association confirms that negative SOI phases indicative of El Niño events is consistently linked to precipitation deficits (lower SPI values) in the region. Conversely, all stations exhibited a robust inverse correlation with the DMI ($p < 0.001$), implying that positive DMI anomalies (Positive IOD) serve as strong drivers of drought conditions throughout Gunungkidul Regency.

However, it must be noted that while these relationships are physically consistent, the monthly time-series data may contain autocorrelation, suggesting that the reported statistical significance levels should be interpreted with caution.

The SPI values of the BPP Panggang, BPP Paliyan, BPP Patuk, BPP Playen, BPP Wonosari, BPP Karangmojo, BPP Semanu, BPP Rongkop, and BPP Saptosari have a moderate association with SOI and DMI values. The SOI and SPI values of the BPP Ponjong, BPP Tepus, BPP Nglipar, and BPP Ngawen have weak and moderate correlations with the DMI values, respectively. The SPI value BPP Semin has a very weak correlation with the SOI and DMI values. The SPI value BPP Gedangsari shows a moderate correlation with the DMI value but does not correlate with the SOI value.

March-April-May (MAM) is the onset of the development of El Nino (Harrison & Larkin, 1998). In 1997/1998, El Nino started to develop in March. Furthermore, El Nino occurs during the positive phase of the IOD. A three-month average was used to assess El Nino and IOD **(Fig. 3-4)**. The three month average was DJF (December – January – February), MAM (March – April – May), JJA (June – July – August), and SON (September – October – November). Meteorological drought associated with El Nino and Positive IOD, indicates to have occurred in 1997/1998 at an elevation of 200 - 400 masl. Then, at elevations of 400 – 600 masl, 0 – 200 masl, and 600 – 800 masl. Drought will worsen as increases elevation, as seen in MAM 1997 and SON 1997.

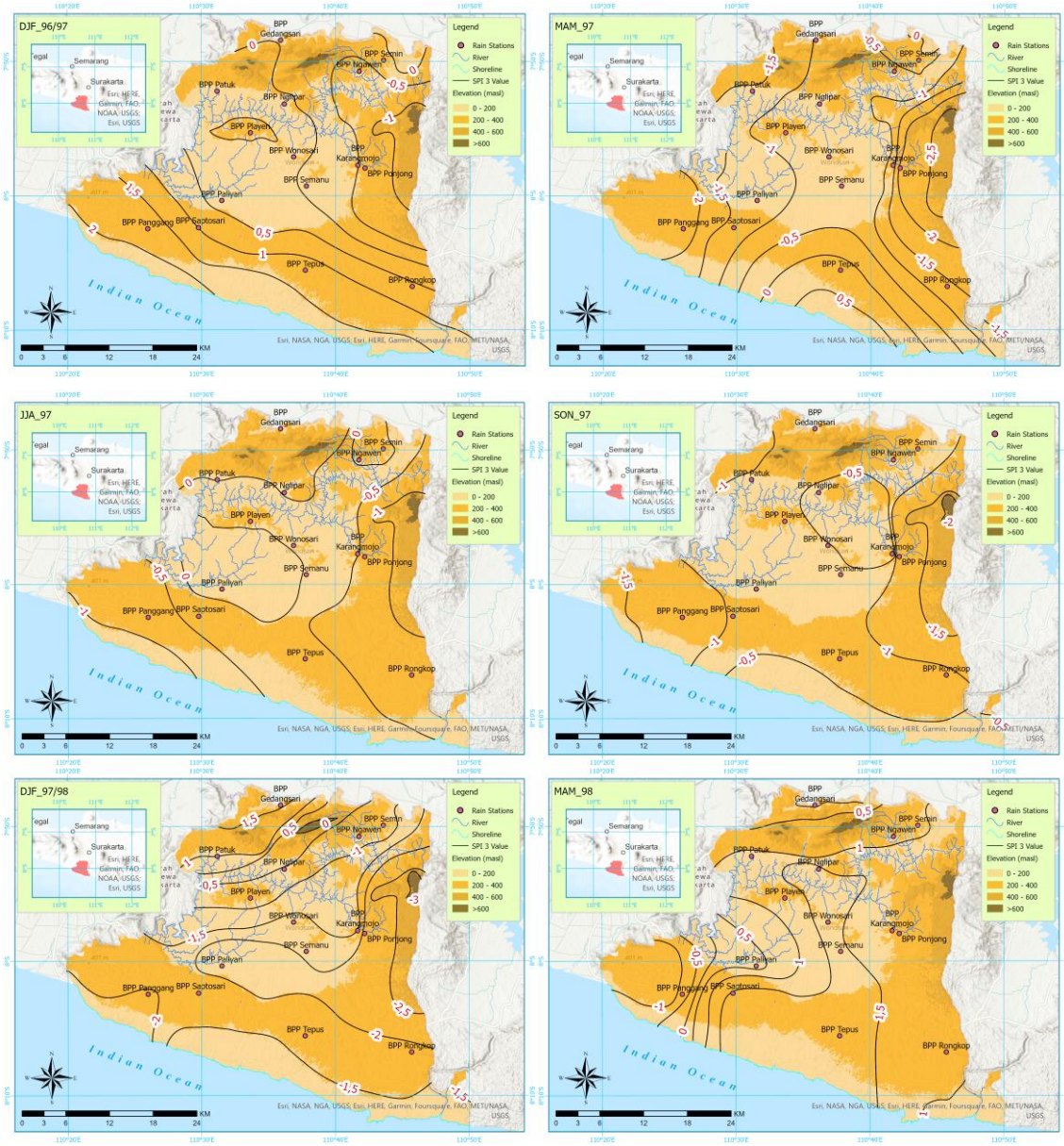

Fig. 3-4 SPI 3 value during meteorological drought, El Nino, and positive IOD in 1997/1998

4 CONCLUSION

Gunungkidul Regency suffered meteorological drought at least 72 times for SPI 3 and 93 times for SPI 12 between 1991 – 2020. The average duration of drought in Gunungkidul Regency is 5 months (SPI 3) and 22 months (SPI 12). Furthermore, the average drought magnitude during the past 30 years for SPI 3 and SPI 12 is -5.33 and -26.29, respectively. Drought intensity in Gunungkidul Regency averages -1.14 for SPI 3 and -1.17 for SPI 12. According to the average SPI 12 values for 1991 – 2020, drought tends to occur at an altitude of 200 – 400 masl.

The SOI and SPI 3 have a positive correlation, whereas the DMI and SPI 3 have a negative correlation. The severe meteorological drought in Gunungkidul Regency increases if El Nino and IOD phases are positive continuously. This illustrates the spatial pattern of SPI 3 values from December 1996 and May 1998, along with the positive IOD and El Nino occurrences in 1997/1998. The meteorological drought trend occurred in areas with elevation of 200 – 400 masl during El Nino and IOD positive events in 1997/1998.

REFERENCES

Abdulrazzaq, Z. T., Hasan, R. H., & Aziz, N. A. (2019). Integrated TRMM Data and Standardized Precipitation Index to Monitor the Meteorological Drought. *Civil Engineering Journal*, *5*(7), 1590–1598. https://doi.org/10.28991/cej-2019-03091355

Agustina, L., Virgianto, R. H., & Fitrianto, A. N. (2021). Utilization of remote sensing data for mapping the effect of Indian Ocean Dipole (IOD) and El Nino Southern Oscillation (ENSO) in Sumatra Island. *IOP Conference Series: Earth and Environmental Science*, *893*(1), 12062. https://doi.org/10.1088/1755-1315/893/1/012062

Ali, M. G., Younes, K., Esmaeil, A., & Fatemeh, T. (2011). Assessment of geostatistical methods for spatial analysis of SPI and EDI drought indices. *World Applied Sciences Journal*, *15*(4), 474–482.

Amirudin, A. A., Salimun, E., Tangang, F., Juneng, L., & Zuhairi, M. (2020). Differential Influences of Teleconnections from the Indian and Pacific Oceans on Rainfall Variability in Southeast Asia. *Atmosphere*, *11*(9). https://doi.org/10.3390/atmos11090886

Anandharuban, P., & Elango, L. (2021). Spatio-temporal analysis of rainfall, meteorological drought and response from a water supply reservoir in the megacity of Chennai, India. *Journal of Earth System Science*, *130*(1). https://doi.org/10.1007/s12040-020-01538-2

Arabameri, A., Chandra Pal, S., Santosh, M., Chakrabortty, R., Roy, P., & Moayedi, H. (2022). Drought risk assessment: integrating meteorological, hydrological, agricultural and socio-economic factors using ensemble models and geospatial techniques. *Geocarto International*, *37*(21), 6087–6115. https://doi.org/10.1080/10106049.2021.1926558

Araneda-Cabrera, R. J., Bermudez, M., & Puertas, J. (2021). Revealing the spatio-temporal characteristics of drought in Mozambique and their relationship with large-scale climate variability. *Journal of Hydrology: Regional Studies*, *38*, 100938. https://doi.org/https://doi.org/10.1016/j.ejrh.2021.100938

Austin, K. F., Noble, M. D., & Berndt, V. K. (2021). Drying Climates and Gendered Suffering: Links Between Drought, Food Insecurity, and Women's HIV in Less-Developed Countries. *Social Indicators Research*, *154*(1), 313–334. https://doi.org/10.1007/s11205-020-02562-x

Bagale, D., Sigdel, M., & Aryal, D. (2021). Drought Monitoring over Nepal for the Last Four Decades and Its Connection with Southern Oscillation Index. In *Water* (Vol. 13, Number 23). https://doi.org/10.3390/w13233411

Bhunia, P., Das, P., & Maiti, R. (2020). Meteorological Drought Study

Through SPI in Three Drought Prone Districts of West Bengal, India. *Earth Systems and Environment*, *4*(1), 43–55. https://doi.org/10.1007/s41748-019-00137-6

BIG. (2018). *DEMNAS - Seamles Digital Elevation Model (DEM) dan Batimetri Nasional*.

Bong, C. H. J., & Richard, J. (2020). Drought and Climate Change Assessment Using Standardized Precipitation Index (SPI) for Sarawak River Basin. *Journal of Water and Climate Change*, *11*(4), 956–965.

Cahyarini, S. Y., Pfeiffer, M., Reuning, L., Liebetrau, V., Dullo, W.-Chr., Takayanagi, H., Anwar, I. P., Utami, D. A., Garbe-Schönberg, D., Hendrizan, M., & Eisenhauer, A. (2021). Modern and sub-fossil corals suggest reduced temperature variability in the eastern pole of the Indian Ocean Dipole during the medieval climate anomaly. *Scientific Reports*, *11*(1), 14952. https://doi.org/10.1038/s41598-021-94465-1

Caloiero, T., Caroletti, G. N., & Coscarelli, R. (2021). IMERG-Based Meteorological Drought Analysis over Italy. *Climate*, *9*(4). https://doi.org/10.3390/cli9040065

Carrière, S. D., Martin-StPaul, N. K., Cakpo, C. B., Patris, N., Gillon, M., Chalikakis, K., Doussan, C., Olioso, A., Babic, M., & Jouineau, A. (2020). The Role of Deep Vadose Zone Water in Tree Transpiration During Drought Periods in Karst Settings–Insights from Isotopic Tracing and Leaf Water Potential. *Science of the Total Environment*, *699*, 134332.

de Silva, R. P., Dayawansa, N. D. K., & Ratnasiri, M. D. (2007). *A comparison of methods used in estimating missing rainfall data*.

Din, M. S. U., Mubeen, M., Hussain, S., Ahmad, A., Hussain, N., Ali, M. A., el Sabagh, A., Elsabagh, M., Shah, G. M., Qaisrani, S. A., Tahir, M., Javeed, H. M. R., Anwar-ul-Haq, M., Ali, M., & Nasim, W. (2022). *World Nations Priorities on Climate Change and Food Security BT - Building Climate Resilience in Agriculture: Theory, Practice and Future Perspective* (W. N. Jatoi, M. Mubeen, A. Ahmad, M. A. Cheema, Z. Lin, & M. Z. Hashmi, Eds.; pp. 365–384). Springer International Publishing. https://doi.org/10.1007/978-3-030-79408-8_22

Djerbouai, S. (2022). Missing Precipitation Data Estimation Using Long Short-Term Memory Deep Neural Networks. *Journal of Ecological Engineering*, *23*(5), 216–225. https://doi.org/10.12911/22998993/147322

Du, C., Chen, J., Nie, T., & Dai, C. (2022). Spatial–temporal changes in meteorological and agricultural droughts in Northeast China: change patterns, response relationships and causes. *Natural Hazards*, *110*(1), 155–173. https://doi.org/10.1007/s11069-021-04940-1

Elhoussaoui, A., Zaagane, M., & Benaabidate, L. (2021). Comparison of various drought indices for assessing drought status of the Northern Mekerra watershed, Northwest of Algeria. *Arabian Journal of Geosciences*, *14*(10), 915. https://doi.org/10.1007/s12517-021-07269-y

Emmanuel, I. (2022). Linkages between El Niño-Southern Oscillation (ENSO) and precipitation in West Africa regions. *Arabian Journal of Geosciences*, *15*(7), 675. https://doi.org/10.1007/s12517-022-09942-2

Evans, J. D. (1996). *Straightforward statistics for the behavioral sciences.* Thomson Brooks/Cole Publishing Co.

Feng, P., Wang, B., Macadam, I., Taschetto, A. S., Abram, N. J., Luo, J.-J., King, A. D., Chen, Y., Li, Y., Liu, D. L., Yu, Q., & Hu, K. (2022). Increasing dominance of Indian Ocean variability impacts Australian wheat yields. *Nature Food*, *3*(10), 862–870. https://doi.org/10.1038/s43016-022-00613-9

Ford, D. C., & Williams, P. W. (1989). *Karst Geomorphology and Hydrology* (1st ed., Vol. 601). Unwin Hyman London.

Garbrecht, J., & Fernandez, G. P. (1994). VISUALIZATION OF TRENDS AND FLUCTUATIONS IN CLIMATIC

RECORDS1. *JAWRA Journal of the American Water Resources Association*, *30*(2), 297–306. https://doi.org/https://doi.org/10.1111/j.1752-1688.1994.tb03292.x

Harrison, D. E., & Larkin, N. K. (1998). El Niño-Southern Oscillation sea surface temperature and wind anomalies, 1946–1993. *Reviews of Geophysics*, *36*(3), 353–399. https://doi.org/https://doi.org/10.1029/98RG00715

Haryono, E., Adji, T. N., Cahyadi, A., Widyastuti, M., Listyaningsih, U., & Sulistyowati, E. (2022). Groundwater and livelihood in Gunungsewu karst area, Indonesia. In *Groundwater for Sustainable Livelihoods and Equitable Growth* (pp. 1–23). CRC Press.

Huang, Y., Zhang, X., Zhang, D., Zhang, L., Zhang, W., Ren, C., Pan, T., Chu, Z., & Chen, Y. (2021). Spatial-Temporal Characteristics of Arctic Summer Climate Comfort Level in the Context of Regional Tourism Resources from 1979 to 2019. In *Sustainability* (Vol. 13, Number 23). https://doi.org/10.3390/su132313056

Jenifer, M. A., & Jha, M. K. (2021). Assessment of precipitation trends and its implications in the semi-arid region of Southern India. *Environmental Challenges*, *5*, 100269. https://doi.org/https://doi.org/10.1016/j.envc.2021.100269

Khoi, D. N., Sam, T. T., Loi, P. T., Hung, B. V., & Nguyen, V. T. (2021). Impact of climate change on hydro-meteorological drought over the Be River Basin, Vietnam. *Journal of Water and Climate Change*, *12*(7), 3159–3169. https://doi.org/10.2166/wcc.2021.137

Kurniadi, A., Weller, E., Min, S.-K., & Seong, M.-G. (2021). Independent ENSO and IOD impacts on rainfall extremes over Indonesia. *International Journal of Climatology*, *41*(6), 3640–3656. https://doi.org/https://doi.org/10.1002/joc.7040

Lestari, D. O., Sutriyono, E., & Iskandar, I. (2018). Respective Influences of Indian Ocean Dipole and El Niño-Southern Oscillation on Indonesian Precipitation. *Journal of Mathematical & Fundamental Sciences*, *50*(3).

Li, H., Zhang, J., Wang, X., Zhu, Y., Liu, L., Wang, B., Zhang, X., Wei, Q., Ding, R., Xuan, J., Shou, L., Zhou, F., & Chen, J. (2022). Robust Subsurface Biological Response During the Decaying Stage of an Extreme Indian Ocean Dipole in 2019. *Geophysical Research Letters*, *49*(16), e2022GL099721. https://doi.org/https://doi.org/10.1029/2022GL099721

Li, J., Garshick, E., Huang, S., & Koutrakis, P. (2021). Impacts of El Niño-Southern Oscillation on surface dust levels across the world during 1982–2019. *Science of The Total Environment*, *769*, 144566. https://doi.org/https://doi.org/10.1016/j.scitotenv.2020.144566

Maharani, D., Sudomo, A., Swestiani, D., Murniati, Sabastian, G. E., Roshetko, J. M., & Fambayun, R. A. (2022). Intercropping Tuber Crops with Teak in Gunungkidul Regency, Yogyakarta, Indonesia. *Agronomy*, *12*(2). https://doi.org/10.3390/agronomy12020449

Maybank, J., Bonsai, B., Jones, K., Lawford, R., O'Brien, E. G., Ripley, E. A., & Wheaton, E. (1995). Drought as a natural disaster. *Atmosphere - Ocean*, *33*(2), 195–222. https://doi.org/10.1080/07055900.1995.9649532

Mazhar, N., & Nawaz, M. (2014). Precipitation data interpolation for meteorological drought mapping in Pakistan. *Pakistan Journal of Science*, *66*(4), 356.

McKee, T. B., Doesken, N. J., & Kleist, J. (1993). The relationship of drought frequency and duration to time scales. *Proceedings of the 8th Conference on Applied Climatology*, *17*(22), 179–183.

Mohamed Salleh, M. K., Ahmad Radib, N. F., & Mohd Amin, N. A. (2021). Spatial Interpolation for Missing Rainfall Data in Northern Region of Peninsular Malaysia. *Journal of Physics: Conference Series*, *1863*(1), 12049. https://doi.org/10.1088/1742-6596/1863/1/012049

Mohseni Saravi, M., Safdari, A. A., & Malekian, A. (2009). Intensity-Duration-Frequency and spatial analysis of droughts using the Standardized Precipitation Index. *Hydrology and Earth System Sciences Discussions*, *6*(2), 1347–1383.

Mubarrok, S., & Jang, C. J. (2022). Annual Maximum Precipitation in Indonesia and Its Association to Climate Teleconnection Patterns: An Extreme Value Analysis. *SOLA*, *18*, 187–192. https://doi.org/10.2151/sola.2022-030

Narulita, I., Fajary, F. R., Syahputra, M. R., Kusratmoko, E., & Djuwansah, M. R. (2021). Spatio-temporal rainfall variability of equatorial small island: case study Bintan Island, Indonesia. *Theoretical and Applied Climatology*, *144*(1), 625–641. https://doi.org/10.1007/s00704-021-03527-x

Nugroho, A. R., Tamagawa, I., & Harada, M. (2021). The Relationship between River Flow Regimes and Climate Indices of ENSO and IOD on Code River, Southern Indonesia. *Water*, *13*(10). https://doi.org/10.3390/w13101375

Nurdiati, S., Sopaheluwakan, A., & Septiawan, P. (2022). Joint Pattern Analysis of Forest Fire and Drought Indicators in Southeast Asia Associated with ENSO and IOD. *Atmosphere*, *13*(8). https://doi.org/10.3390/atmos13081198

Odériz, I., Silva, R., Mortlock, T. R., & Mori, N. (2020). El Niño-Southern Oscillation Impacts on Global Wave Climate and Potential Coastal Hazards. *Journal of Geophysical Research: Oceans*, *125*(12), e2020JC016464. https://doi.org/https://doi.org/10.1029/2020JC016464

Oliveira, R. S., Eller, C. B., Barros, F. de v, Hirota, M., Brum, M., & Bittencourt, P. (2021). Linking plant hydraulics and the fast–slow continuum to understand resilience to drought in tropical ecosystems. *New Phytologist*, *230*(3), 904–923. https://doi.org/https://doi.org/10.1111/nph.17266

Qaisrani, Z. N., Nuthammachot, N., Techato, K., & Asadullah. (2021). Drought monitoring based on Standardized Precipitation Index and Standardized Precipitation Evapotranspiration Index in the arid zone of Balochistan province, Pakistan. *Arabian Journal of Geosciences*, *14*(1), 11. https://doi.org/10.1007/s12517-020-06302-w

Rahayu, L., Rozaki, Z., Indardi, & Isdiana, A. (2022). Adaptation of red rice farmers to long drought in Ponjong Districts Gunung Kidul Regency, Yogyakarta Indonesia. *IOP Conference Series: Earth and Environmental Science*, *1016*(1), 12040. https://doi.org/10.1088/1755-1315/1016/1/012040

Raut, S., Modiri, S., Heinkelmann, R., Balidakis, K., Belda, S., Kitpracha, C., & Schuh, H. (n.d.). *Investigating the Relationship Between Length of Day and El-Niño Using Wavelet Coherence Method* (pp. 1–6). Springer Berlin Heidelberg. https://doi.org/10.1007/1345_2022_167

Ropelewski, C. F., & Halpert, M. S. (1989). Precipitation patterns associated with the high index phase of the Southern Oscillation. *Journal of Climate*, 268–284.

Saini, D., Singh, O., Sharma, T., & Bhardwaj, P. (2022). Geoinformatics and analytic hierarchy process based drought vulnerability assessment over a dryland ecosystem of north-western India. *Natural Hazards*, *114*(2), 1427–1454. https://doi.org/10.1007/s11069-022-05431-7

Saji, N. H., Goswami, B. N., Vinayachandran, P. N., & Yamagata, T. (1999). A dipole mode in the tropical Indian Ocean. *Nature*, *401*(6751), 360–363.

Saji, N. H., & Yamagata, T. (2003). Possible impacts of Indian Ocean dipole mode events on global climate. *Climate Research*, *25*(2), 151–169.

Salimi, H., Asadi, E., & Darbandi, S. (2021). Meteorological and hydrological drought monitoring using several drought indices. *Applied Water Science*, *11*(2), 11.

https://doi.org/10.1007/s13201-020-01345-6

Shi, H., Zhou, Z., Liu, L., & Liu, S. (2022). A global perspective on propagation from meteorological drought to hydrological drought during 1902–2014. *Atmospheric Research*, *280*, 106441. https://doi.org/10.1016/j.atmosres.2022.106441

Siswanto, S., Wardani, K. K., Purbantoro, B., Rustanto, A., Zulkarnain, F., Anggraheni, E., Dewanti, R., Nurlambang, T., & Dimyati, M. (2022). Satellite-based meteorological drought indicator to support food security in Java Island. *PLOS ONE*, *17*(6), e0260982. https://doi.org/10.1371/journal.pone.0260982

Sudaryatno. (2016). Drought Vulnerability Mapping with Geomorphological Approach in Yogyakarta Special Region (DIY) and Central Java. *IOP Conference Series: Earth and Environmental Science*, *47*(1), 12023. https://doi.org/10.1088/1755-1315/47/1/012023

Suhartanto, E., Wahyuni, S., & Mufadhal, K. M. (2021). Estimation of Rainfall from Climatology Data Using Artificial Neural Networks in Palembang City South Sumatera. *IOP Conference Series: Earth and Environmental Science*, *930*(1), 12062. https://doi.org/10.1088/1755-1315/930/1/012062

Tladi, T. M., Ndambuki, J. M., & Salim, R. W. (2022). Meteorological drought monitoring in the Upper Olifants sub-basin, South Africa. *Physics and Chemistry of the Earth, Parts A/B/C*, 103273. https://doi.org/10.1016/j.pce.2022.103273

Tora, T. T., Degaga, D. T., & Utallo, A. U. (2021). Drought vulnerability perceptions and food security status of rural lowland communities: An insight from Southwest Ethiopia. *Current Research in Environmental Sustainability*, *3*, 100073. https://doi.org/https://doi.org/10.1016/j.crsust.2021.100073

Trenberth, K. E. (1984). Signal versus noise in the Southern Oscillation. *Monthly Weather Review*, *112*(2), 326–332.

Wang, W., Wang, J., & Romanowicz, R. (2021). Uncertainty in SPI Calculation and Its Impact on Drought Assessment in Different Climate Regions over China. *Journal of Hydrometeorology*, *22*(6), 1369–1383. https://doi.org/10.1175/JHM-D-20-0256.1

Wang, Z., Wu, R., Huang, K., Qiu, Y., Li, Z., Lv, Y., & Wan, J. (2022). Structure identification of a karst groundwater system based on high-resolution rainfall-hydrological response characteristics. *Environmental Science and Pollution Research*, *29*(18), 26922–26935. https://doi.org/10.1007/s11356-021-17880-x

WMO. (2006). Drought monitoring and early warning: concepts, progress and future challenges. *World Meteorological Organization*, *1006*.

Wu, J., Chen, X., Yao, H., & Zhang, D. (2021). Multi-timescale assessment of propagation thresholds from meteorological to hydrological drought. *Science of The Total Environment*, *765*, 144232. https://doi.org/https://doi.org/10.1016/j.scitotenv.2020.144232

Yildirim, G., & Rahman, A. (2022). Spatiotemporal meteorological drought assessment: a case study in south-east Australia. *Natural Hazards*, *111*(1), 305–332. https://doi.org/10.1007/s11069-021-05055-3

Yildirim, G., Rahman, A., & Singh, V. P. (2022). Meteorological and hydrological drought hazard, frequency and propagation analysis: A case study in southeast Australia. *Journal of Hydrology: Regional Studies*, *44*, 101229. https://doi.org/https://doi.org/10.1016/j.ejrh.2022.101229

Yin, H., Wu, Z., Fowler, H. J., Blenkinsop, S., He, H., & Li, Y. (2022). The Combined Impacts of ENSO and IOD on Global Seasonal Droughts. In *Atmosphere* (Vol. 13, Number 10). https://doi.org/10.3390/atmos13101673

Yulihastin, E., Putranto, M. F., & Suaydhi. (2021). The Effect of Local

Forcing on Anomalously High Rainfall during Dry Season in Java, Indonesia. *Journal of Southwest Jiaotong University*, *56*(3), 32–42. https://doi.org/10.35741/issn.0258-2724.56.3.3

Zhang, Y., Zhou, W., Wang, X., Chen, S., Chen, J., & Li, S. (2022). Indian Ocean Dipole and ENSO's mechanistic importance in modulating the ensuing-summer precipitation over Eastern China. *Npj Climate and Atmospheric Science*, *5*(1), 48. https://doi.org/10.1038/s41612-022-00271-5